Numerical simulation of polymer nanocomposites using a self-consistent mean-field model

Kim, K.; Utracki, L. A.; Kamal, M. R.

Publisher's version / Version de l'éditeur:
https://doi.org/10.1063/1.1794636
The Journal of Chemical Physics, 121, 21, pp. 10766-10777, 2004-12-01

Numerical simulation of polymer nanocomposites using self-consistent mean-field model

K. Kim[a)]
Department of Chemical Engineering, McGill University, Montreal, Québec H3A 2B2, Canada and National Research Council of Canada, Industrial Materials Institute, Boucherville, Québec J4B 6Y4, Canada

L. A. Utracki
National Research Council of Canada, Industrial Materials Institute, Boucherville, Québec J4B 6Y4, Canada

M. R. Kamal
Department of Chemical Engineering, McGill University, Montreal, Québec H3A 2B2, Canada

(Received 18 June 2004; accepted 26 July 2004)

Clay-containing polymeric nanocomposites (PNC) are mixtures of dispersed clay platelets in a polymeric matrix. These materials show enhancement of physical properties, such as modulus, strength, and dimensional stability, as well as a reduction of gas permeability and flammability. The performance is related to the degree of clay dispersion (i.e., intercalation or exfoliation) and the bonding between the clay and the matrix. The main goal of this work has been to map the degree of dispersion as a function of independent variables (viz., magnitude of the interaction parameters, molecular weights, composition, etc.). In this paper, we present the results of the numerical analysis of the equilibrium thermodynamic miscibility using one- and two-dimensional (1D and 2D) models based on the self-consistent mean-field theory. In the limit, the 2D model reproduced the 1D model published results. The adopted 2D model considers the presence of four PNC components: solid clay platelets, low molecular weight intercalant, polymeric matrix, and end-functionalized compatibilizer. The simulations, with realistic values of the binary interaction parameters, were analyzed for potential exfoliation of PNC with a polyolefin as the matrix. The simulation results show that intercalation and exfoliation is expected within limited ranges of the independent variables. The presence of a bare clay surface (e.g., generated by thermal decomposition of intercalant or extraction by molten polymer) has a strong negative effect on the dispersion process. The simulation successfully identified the most influential factors, e.g., optimum ranges of the compatibilizer and the intercalant concentration. © *2004 American Institute of Physics.*
[DOI: 10.1063/1.1794636]

I. INTRODUCTION

Polymer performance may be significantly improved by the addition of inorganic clay. In particular, the modulus, hardness, tensile strength, heat deflection temperature, flammability, and barrier properties are likely to be enhanced.[1] The clay dispersion process has been modeled considering the thermodynamics,[2–10] kinetics,[11–20] and continuum mechanics.[21,22]

Unlike conventional composites, polymeric nanocomposites (PNC) usually contain less than 5 vol % of solid reinforcement. For equivalent mechanical performance, PNC have significantly lower densities than traditional composites, e.g., with 30–50 wt % glass fiber or mineral filler. The advantages originate from the nature of the layered inorganic fillers and from their nanodispersion. However, these promising characteristics are difficult to achieve owing to problems in reproducibly obtaining exfoliation of the clay. Furthermore, to achieve PNC superiority over conventional composites, it is necessary to ascertain that are dispersion of clay platelets within the polymer matrix is stable during the postdispersion forming processes, i.e., that the system is thermally and thermodynamically stable. Thus, the preparation of PNC must satisfy the following three basic criteria: (i) optimized morphology, (ii) stability of morphology during processing, and (iii) adequate stress transfer between phases in the solid state.

In the recent years, molecular simulation methods, such as molecular mechanics (MM) simulations [based on molecular dynamics(MD)] have been applied to investigate the diverse properties of polymeric systems in terms of energetics and kinetics.[23,24] The MM methods adopt several chain models, viz., freely jointed or rotating chain, rotational isometric state, nonentangled Rouse-type,[25,26] highly entangled reptation-type,[27] and hydrodynamic Zimm model.[28]

Molecular simulation fills the gap between theory and experiment. It has been used to conduct mathematical ''experiments,'' to analyze the influence of individual components and/or parameters, and to optimize the system. Consequently, molecular simulation has become a powerful tool in polymer science and technology, complementing the theories and experiments. However, molecular simulation is limited

a)Author to whom correspondence should be addressed. Electronic mail: dimazio71@empas.com

on the space and time scales as it deals with relatively few molecules in the system. As an alternative, coarse-grained models have been developed. These lump a number of molecules or mers into a single grain and then compute the performance of PNO,[11–14,18] polymer blends, or block copolymers.[29,30] With growing frequency, MD simulations are being used to solve practical industrial problems. One of the fascinating features is that the method can be used in conjunction with different length-scale methods via multiscale modeling.[31]

Alternative methodologies have been suggested to overcome the limitations of space and time. The lattice models based on statistical mechanics have been successful in this regard. Here, polymer chains are represented by random walks on numerical lattices, and thus, many states can be generated and equilibrated. Lattice models are widely used for classical liquids, polymer solutions, melts, as well as blends.[32] However, they do not consider the detailed molecular structure. Despite this limitation, lattice modeling can be advantageous because the infinite number of conformations of real chains in continuum space is reduced to a finite number, which makes computing feasible. Furthermore, the average number of contact interactions is relatively easy to evaluate. Initially, Vaia and Giannelis[4,5] adopted a lattice approach to study the interactions between macromolecules and the organically modified clays. In their work, the matrix within the organoclay-polymer-organoclay sandwich was a monodispersed homopolymer.

The advantages of the self-consistent mean-field (SCF) model[33–42] over the classical lattice approach are well described in a series of publications by Balazs and co-workers.[6–9] The model used in the SCF calculations consists of two infinite parallel platelets immersed in a bath of molten polymer. To incorporate the concentration effects, Ginzburg *et al.* hybridized the SCF one-dimensional (1D) model with the density functional theory (DFT) for intercalant-grafted clay platelets, 1-nm thick and with a 30-nm diameter, dispersed in a polymer.[10] Numerical[36,37] and analytical SCF methods[38,39] have been successfully used for describing the adsorption of simple molecules[2,3] or block copolymers,[33–35] the interactions between the hairy surface and the free polymer,[36] as well as the behavior of the end-attached macromolecular chains to a solid surface. The numerical approach was verified by comparison with the SCF analytical theory, and good agreement was reported.[39] Rigorous computations were carried out to obtain a complete description of the lattice polymer fluids and polymer solutions.[40,41] The method was also effective in handling complex inhomogeneous liquids.[42] More recently, the SCF model was used to interpret continuum quantities such as stress[43] and viscoelasticity of the inhomogeneous dense polymer systems.[44]

In an industrial environment, PNC formation may be accomplished by following one of the three principal methods: (i) chemical (dispersing organoclay in a monomer then polymerizing it), (ii) solution (dispersing organoclay in polymer solution then removing the solvent), and (iii) melt compounding of organoclay with polymer.[1] Irrespective of which method is used, PNC formation into a finished product is accompanied by mixing/compounding, which requires additional energy (shear or elongation) input. The PNC performance intimately depends on all these three components: thermodynamics, kinetics, and processing.

The work described in this paper focuses only on the equilibrium thermodynamics. It attempts to answer questions regarding the miscibility of ingredients and the stability of morphology under processing conditions. Time and mixing effects are neglected, as is the thermal stability, polydispersity of polymer molecular weight (MW), and that of clay platelet size and shape. The systems considered comprise four species: clay, intercalant, end-terminated compatibilizer, and host polymer. The ''miscibility'' term is used here to indicate the net energy gain during the dispersion process, expressed by the negative value of the free energy of mixing.

In the proposed PNC model, some modifications are made to earlier representations.[4,6,20] As before,[6,9] it assumes that two parallel clay platelets are placed in a reservoir of molten polymer in the x-y plane, and the distance between them in the z direction may vary. A single polymer chain is modeled as N_k number of Kuhn segments, whose length is given by l_k. Thus, the MW of a macromolecule is proportional to $N_k \times l_k$. Unlike the molecular theory, which deals with the individual molecules in the system, the theory based on Kuhn segment alleviates the computational requirement without loss of generality. The number and size of the Kuhn segments depend on the type of monomer and on MW. For example, for polyethylene (PE) and polypropylene (PP), the number of mers per Kuhn segment are $N_k = 8.2$ and 6.5, respectively,[45] equivalent to the segmental mass, $M_k = 230$ and 272. This means that the cell size of the SCF lattice is significantly larger than that in the classical lattice theories, where the statistical segment is identified with either one mer or with its fraction per one C atom of the main chain. Accordingly, in this work, the lattice cell may be subdivided, i.e., one cell may be occupied by several species or void (free volume). However, the sum of all the specie fractions in a cell must be 1. This approach results in a significant reduction of the computing time without loss of precision.

The grafting density of the platelets with short paraffinic intercalant chains (''surfactants'' in the literature[6]) can vary from 0% to 100% coverage. Furthermore, the polymer melt contains different amounts of end-functionalized macromolecules of different chain lengths, comparable to that in industrial processes. Due to the clay surface effects, the mobility of a macromolecule decreases as it moves away from the bulk region. The chain mobility is related to the local vacancy fraction (free volume), which is assumed to obey a truncated power-law distribution, with two flat plateaux near the solid plate ($z = 0$) and the bulk region ($z = \infty$). Two types of binary interactions are considered, the long-range-type between two clay platelets (van der Waals and electrostatic), and the short-range described in the classical van Laar, Huggins, or Flory theory. The former is incorporated through the Hamaker equation, whereas the latter is through the binary interaction parameters χ_{ij}. Temperature effects enter the calculations directly as thermal energy units ($k_B T$) and through the temperature-dependent χ_{ij}.

The main goal of this work is to identify the process

variables that affect the platelet dispersion in a polymeric matrix. In short, the aim is to map the degree of dispersion as a function of the independent variables, viz., the magnitude of the interaction parameters, molecular weight, the presence of bare solid surface, composition, etc. The computation employs realistic values of the interaction parameters for liquid-liquid[1] and solid-solid interactions.[46,47] The treatment is valid for any polymer matrix, but considering the industrial importance, the selected values of the parameters primarily address PNC with a polyolefin (PP or PE) matrix.

II. FORMULATION

The numerical implementation is based on the SCF theory developed by Fleer *et al.*[3] The methodology is adopted to simulate realistically the physical situation involving PNC. Balazs *et al.* have extended the classical SCF approach to investigate the thermodynamic aspects of PNC.[6] The authors assumed that the clay platelets are fully covered by the intercalant; thus, the solid-solid interactions between the clay surfaces were irrelevant. The current approach assumes the presence of different interactions including solid-solid, solid-liquid, and liquid-liquid type. Only binary-type and short- and long-range interactions are considered. Since the method is well established in the seminal text[3] and the papers that followed,[6–9,33–42] detailed information on the model and computational formalism can be found there. The new elements introduced in this work are the presence of the four components simulating the polyolefin-based PNC (with the appropriate values of the binary interaction parameters), consideration of solid clay surface, as well as the two-dimensional (2D) computations.

The physical space is assumed to involve a statistical lattice divided into M_x and M_z layers in the x and z directions, thus averaging in the y direction (see Fig. 1). The clay platelet is partially covered by a low molecular weight intercalant (surfactant or an organic modifier), whose molecular weight and grafting density are denoted by N_o and ρ_o, respectively. The rest of the platelet is either bare or covered by a compatibilizer or host polymer. The bare surface fraction is given as ρ_v. The compatibilizer considered in this work is an end-functionalized macromolecular chain having repeating units of the backbone chain chemically similar or identical to those of the host polymer. The molecular weight and grafting density of the compatibilizer are given as N_g and ρ_g, whereas those of the host polymer are given as N_h and ρ_h, respectively. Note that the subscripts h, g, o, s, and v, respectively, denote the host polymer, grafted polymer (compatibilizer), intercalant (organic modifier), inorganic solid surface, and vacancy. From the given densities (expressing the local specimen volume fraction), the surface-grafted amount for each species can be determined by $\theta_i = N_i \times \rho_i$.[37] Within the first z layer, the grafting densities for the intercalant and the grafted polymer represent the number of molecules attached to the clay surface (per unit area). Unlike other constituents, the host polymer does not chemically bond to the solid platelet thus, the density of the host polymer in the vicinity of the solid wall is calculated as $\rho_h = 1-(\rho_o+\rho_g+\rho_v)$. The solid-solid interaction is assumed to prevail only in the bare clay regions where neither the intercalant, compatibilizer, nor host polymer is present. The clay-clay interactions are van der Waals and electrostatic type, thus of the long-range type. In statistical description, a Kuhn freely rotating polymer chain with a number N_k of statistical segments represents a single macromolecule. Depending on the degree of polymerization and chain stiffness, the number of Kuhn segments in a typical industrial polymer ranges from about $N_k = 10$ to 500.[45]

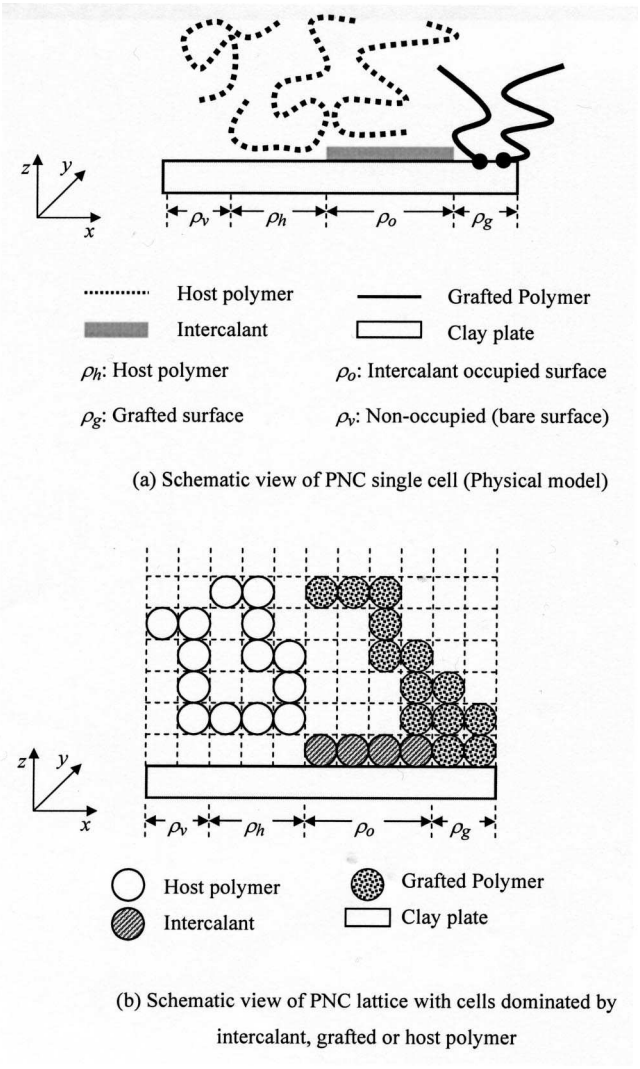

FIG. 1. Schematic view of the physical and modeled systems.

Every lattice layer is occupied by a statistical segment of a host polymer, intercalant, compatibilizer, or a free volume (vacancy). For simplicity, the variation with respect to the lateral dimension y is averaged; thus, the formulation is reduced to 2D, considering the x and z directions only. The fundamental concept of SCF modeling is based on the weighted Markov process, which assumes that the properties in a specific lattice site depend only on the neighboring ones.

The probability function of a monomer-type i of the segment s at (x,z) is given as $G_i(x,z,s)$. The statistical lattice is assumed to be a cube, whose vertex represents the Kuhn length. Index 1 and N_i denote, respectively, the two ends of a statistical chain. The probability of the segments at layer (x,z) is then determined from a recurrence relation. Thus,

the probability function of segment $(s+1)$ is given in terms of the preceding segment s and neighboring layers $z-1$, $z+1$, $x+1$, and $x-1$,

$$G_i(x,z,s+1)=G_i(x,z)[\lambda_1 G_i(x-1,z-1,s)+\lambda_1 G_i(x+1,z-1,s)+\lambda_0 G_i(x,z,s)+\lambda_1 G_i(x-1,z+1,s)+\lambda_1 G_i(x+1,z+1,s)], \quad (1)$$

where λ_1 and λ_0 are coefficients solely dependent on the lattice geometry. For a two-dimensional lattice, $\lambda_1=1/6$ and $\lambda_0=2/6$. The one-dimensional formulation is obtained from Eq. (1) by neglecting x dependence; thus, the one-dimensional coefficients of Eq. (1) are $\lambda_1=1/6$ and $\lambda_0=4/6$. Upon the normalization of the probability function $G_i(x,z,s)$ over the total length of polymer type i, N_i, the previous expression becomes

$$G_i(x,z,s+1)=\sum_{s=1}^{N_i} G_i(x,z,s)\bar{G}_i(x,z,s), \quad (2)$$

where $\bar{G}_i(x,z,s)$ is the neighbor-averaged probability function given by Eq. (1). Two conditional probabilities are introduced for each end located at 1 and N_i. We probability function $G_i(x,z,s|1)$ is the statistical weight of the molecules i ending with the first segment 1, whereas $G_i(x,z,s|N_i)$ is that with the last segment N_i,

$$G_i(x,z,s|1)=\sum_{s=1}^{N_i} G_i(x,z,s)\bar{G}_i(x,z,s+1|1),$$
$$G_i(x,z,s|N_i)=\sum_{s=1}^{N_i} G_i(x,z,N_i)\bar{G}_i(x,z,s-1|N_i). \quad (3)$$

In Eq. (3), the initial condition used to calculate the recurrence relations is provided by the segment-weighting factor expressed by the Boltzmann weighting,

$$G_i(x,z,1|1)=G_i(x,z,1)=\exp\left[-\frac{u_i(x,z)}{k_BT}\right], \quad (4)$$

where k_B is the Boltzmann constant and T denotes the absolute temperature, whereas $u_i(x,z)$ represents the potential for segment type i. The latter has two parts: a hardcore (repulsive) potential $u'(x,z)$ and the contribution stemming from the interactions between participating species, viz., macromolecules segments, intercalant radicals, and inorganic clay platelets,

$$u_i(x,z)=u'(x,z)+k_BT\hat{u}_i(x,z). \quad (5)$$

The hardcore potential $u'(x,z)$ is independent of the species and serves as a space filler for the region where the strong entropic barrier exists, e.g., wall-bounded region or confinement.[33] Contributions to the interaction potential $\hat{u}_i(x,z)$ in Eq. (5) originate from different sources. A classical Flory-Huggins theory is adopted for the estimation of the liquid-liquid and liquid-solid potentials, whereas the long-range van der Waals interaction is assumed to be a solid-solid-type interaction.

$$\text{liquid-liquid:}\quad \hat{u}_i(x,z)=\sum_{(j\neq i)}\chi_{ij}(\langle\phi_j(x,z)\rangle-\phi_j^b), \quad (6)$$

$$\text{liquid-solid:}\quad \hat{u}_i(x,z)=\lambda_1\chi_{is}, \quad (7)$$

$$\text{solid-solid:}\quad \hat{u}(x,z)=\frac{A\epsilon}{12\pi}\frac{\bar{\phi}_v(z)x}{z^2}, \quad (8)$$

where A is the Hamaker constant between a pair of clay platelets, whose gallery is not occupied. The Hamaker constant can be measured[46] or calculated.[47] In this paper, $A=7.80\times10^{-20}$ (J) was used, which is equivalent to 20 k_BT (Boltzmann unit). The superscript b denotes a bulk quantity, and $\bar{\phi}_v(z)$ is an averaged vacancy fraction over the lateral dimension (x). The contribution from Eq. (8) only prevails in the presence of the solid plate $(z=1)$. χ_{ij} is a liquid-liquid-type interaction parameter, whereas χ_{is} (the binary interaction parameters for $j=s$) denote the liquid-solid interaction for $i=h$, g, and o, which refers to the clay interaction with the host polymer, compatibilizer, and intercalant. Ginzburg *et al.* used an exponential function to model a purely attractive and short-ranged pair potential between parallel platelets in a three-component system.[10]

In Eq. (8), ϵ denotes the ratio between the lateral area of the clay platelet and the length of the unit segment. Therefore, the value of ϵ depends on the type of clay as well as the geometrical configuration of the computational domain. Considering the size of the clay platelet and that of the lattice, the value of ϵ ranges from 0 to 20. The full platelet-platelet interaction occurs when $\bar{\phi}_v(z)=1$, i.e., when no organic molecule occupies the surface sites. Long chain macromolecules tend to show low mobility and solidification in the vicinity of the solid wall, which results in a low free volume fraction. At the other limit, the averaged vacancy fraction reaches an asymptotic value in the bulk region.[48] The vacancy distribution in the medium is assumed to obey a truncated power-law-type approximation given by

$$\frac{\bar{\phi}_v(z)-\bar{\phi}_v^{\infty}}{\bar{\phi}_v^0-\bar{\phi}_v^{\infty}}=\left[1-\left(\frac{z-1}{M_z}\right)^n\right]^m, \quad (9)$$

where $\bar{\phi}_v^0$ and $\bar{\phi}_v^{\infty}$ are the averaged vacancy volume fractions at $z=1$ and $z=M_z+1$, respectively; n and m are the characteristic constants that determine the shape of the vacancy distribution. Once the amount of the surfactant and coupling agent in the interlamellar gallery is given, the value of $\bar{\phi}_v^0$ is known, whereas $\bar{\phi}_v^{\infty}$ can be experimentally determined. This expression ensures that there are two flat plateaux, one within a few nanometers of the solid wall and the second within the bulk region. In addition, the slope, as well as the range of the asymptotic vacancy fraction, can be adjusted by changing the characteristic constant. The van der Waals interaction contributes to the unfavorable energy gain against clay exfoliation, whereas the entropy and enthalpy of mixing under attractive binary interactions induce system miscibility.

The term $\langle\phi_i(x,z)\rangle$ in Eq. (6) may be expressed as $\langle\phi_i(x,z)\rangle=[\lambda_1\phi_i(x-1,z-1)+\lambda_1\phi_i(x+1,z-1)+\lambda_0\phi_i\times(x,z)+\lambda_1\phi_i(x-1,z+1)+\lambda_1\phi_i(x+1,z+1)]$. Similarly, as for Eq. (1), the 1D version of the averaged volume

fraction expression can be obtained by neglecting the variations in the x direction. Note that the same rule as Eq. (1) is applied to the coefficients λ_1 and λ_0.[3]

The description of an algorithm to evaluate Eq. (5) is well established.[33,34] Contributions from the liquid-liquid and liquid-solid interactions have been included. The solid-solid interactions ($\chi_{ss}=A\epsilon/12\pi$) are about 100 times stronger than the liquid-liquid interactions, whereas the liquid-solid interactions are dominant only near the solid surface ($z=1$).[1,48] The solid-solid interactions reflect the strong bonding between the crystalline solid surfaces. The intercalant and the end-terminated compatibilizer are designed to attenuate the unfavorable solid-solid bonding. The liquid-solid interaction parameter can be estimated from the Berthelot's geometrical mean rule once the interaction parameters between solid-solid and liquid-liquid are known. Ample work has been devoted to the characterization of these different types of binary interaction parameters for polymer blends[32] and for PNO.[1]

The free energy F is due to two contributions: the entropy due to changes of conformation, S_i, and the enthalpy due to interactions between participating species, H_i, for each component i,

$$F_i(x,z)=H_i(x,z)-TS_i(x,z). \tag{10}$$

As it is the custom, the free energy and its components are expressed in Boltzmann units (k_BT). The combinatorial entropy is given in terms of the species volume fraction and the number of ways that a particular system can be configured,

$$S_i(x,z)=k_B\ln[G_i(x,z)]. \tag{11}$$

The interaction enthalpy for soft materials is given in terms of short-range interactions, which can be replaced by the summation over the nearest neighbors. The three types of interactions are described in Eqs. (6)–(8). Thus, the enthalpy of mixing for liquid-liquid and liquid-solid interactions may be expressed as

$$H_i(x,z)=\sum_j \chi_{ij}\langle\phi_j(x,z)\rangle+\lambda_1\chi_{is}. \tag{12}$$

From Eqs. (11) and (12), the total free energy of segment type i at every x and z location in the system is given by

$$F_i(x,z)=\phi_i(x,z)\left\{\ln[G_i(x,z)]+\sum_{j(\neq i)}\chi_{ij}\langle\phi_j(x,z)\rangle\right\}+\phi_i(x,1)\lambda_1\chi_{is}. \tag{13}$$

Note that the liquid-solid interaction is only limited to $z=1$. Summation over the participating macromolecules, i, (including solid-solid interactions) yields the total excess free energy,

$$F(x,z)=\sum_i \phi_i(x,z)\left\{u_i(x,z)+\sum_{j(\neq i)}\chi_{ij}\langle\phi_j(x,z)\rangle\right\}+\sum_i \phi_i(x,1)\lambda_1\chi_{is}+\frac{A\epsilon}{12\pi}\frac{\bar{\phi}_v(z)x}{z^2}. \tag{14}$$

The excess free-energy difference at a particular gap width H can be calculated by taking the difference between the total free energies when the clay platelets are in close contact and when they are separated by the gallery distance, H.

$$\Delta F(H)=\sum_{z=1}^{H}\sum_{x=1}^{M_z}F(x,z)-\sum_{z=1}^{h_0}\sum_{x=1}^{M_z}F(x,z), \tag{15}$$

where h_0 is an initial gallery height. This conversion from z to H can only be used for the excess free-energy calculation, whereas the other functions, such as free energy and density profiles, do not involve H but x and z as dependent variables.

The volume fraction at a specific segment location s, $\phi_i(x,z,s)$, is a product of two probability functions: the probability of a chain starting at segment 1 and ending with segment s at layer z, and that of a chain starting at segment N_i also ending with segment s at layer z. The total volume fraction of each component, $\phi_i(x,z)$, is calculated by summing the segmental volume fraction $\phi_i(x,z,s)$ over the segments. The volume fraction for the species simply denotes the number of molecules in a unit segment, whereas the density is given per unit area. Note that to determine the set of probability values, the recurrence relation in Eq. 3 is used. Thus,

$$\phi_i(x,z,s)=C_i\frac{G_i(x,z,s|1)G_i(x,z,s|N_i)}{G_i(x,z)}, \tag{16}$$

where C_i is a normalizing constant. The expression for C_i may also be derived from the total number of segments belonging to molecules i between the two plates. In this case,

$$C_i=\left[\sum_{x=1}^{M_x}\sum_{z=1}^{M_z}\phi_i(x,z)\right]\Bigg/\times\left[N_i\sum_{x=1}^{M_x}\sum_{z=1}^{M_z}G_i(x,z,N_i|1)\right]. \tag{17}$$

In the bulk, all G_i's are unity, and therefore, $C_i=\phi_i/N_i$. Equations (16) and (17) are supplemented by the requirement that the total volume fraction within each cell add up to 1,

$$\sum_i \phi_i(x,z)=\sum_i\sum_{s=1}^{N_i}\phi_i(x,z,s)=1. \tag{18}$$

Depending on the type of polymer participating in the system, the initial conditions for the probability functions may vary. For example, there are different initial conditions for each macromolecular end used in the simulation. For both the intercalant and end-grafted compatibilizer, the first segment of the statistical chain is always located on the clay surface. Therefore, if it is either grafted at 1 or L layers, the initial condition for the probability function becomes

$$G(x,z,1|1)=\begin{cases}G(x,1) & \text{when } z=1\\ G(x,L) & \text{when } z=L\\ 0 & \text{otherwise}\end{cases} \tag{19}$$

For the randomly distributed host polymer, the probability function does not have any restriction. Its value is calculated from the initial guess and from the bulk condition,

$$G(x,z,1|1)=G(x,z); \tag{20}$$

thus, $\phi_h(x,z)=1$, $\phi_g(x,z)=$, and $\phi_0(x,z)=0$ when $x=1$, $x=M_x$, or when $z=M_z$.

TABLE I. Parameters used to compute the data presented in Figs. 2–5.

Fig.	N_g	N_o	N_h	ρ_h	ρ_g	ρ_o	ϵ	χ_{hs}	χ_{gs}	χ_{os}
2	50	NA	50–2000	0.95	0.05	NA	NA	0.0	0.0	0.0
3	25–200	NA	200	0.98–0.9	0.02–0.1	NA	NA	0.0	0.0	0.0
4	200	10	400	0.1	0.2	0.7	NA	0–0.01	0–0.01	0–0.02
5	200	10	400	0.05	0.0–0.2	0.5–0.8	0–20	0.01	−0.01	−0.02

Equations (19) and (20) provide the initial conditions for the recurrence calculations according to Eq. (1). Other boundary conditions are readily derived. For 2D computations, a pair of plates is located in the middle of the computational lattice, partly covered either by an intercalant or by a compatibilizer. At both extremes, $x=1$ and $x=M_x$, the bulk conditions prevail. Similarly, in the direction perpendicular to the plate, the bulk conditions apply at $z=M_z$. Thus, the probability function and the volume fraction simply become zero for the end-grafted polymer,

$$G(x,z,1|s)=\begin{cases}0 & \text{when } x=1 \text{ or } M_x\\ 0 & \text{when } z=M_z\end{cases} \tag{21}$$

The algebraic expressions in Eqs. (16)–(18), subjected to the boundary conditions in Eq. (18), are solved using a nonlinear algebraic equation solver.[49] Note that the requirement in Eq. (18) imposes an implicit constraint on the system of equations. Thus, the solution is found by iteration. Initially, the potential function is assumed, and from the guessed potential, the volume fraction and its recurrence relation are computed. The solution of the set of algebraic equations is obtained iteratively until the condition imposed by Eq. (18) is met.

III. RESULTS

In this Section, the results of the computations will be presented. These are based on the formulation described in the preceding part. The number of statistical (Kuhn) segments of the macromolecules used in these calculations varies from 10 to 2000, and the values of the other parameters used to compute the data presented in Figs. 2–5 are listed in Table I.

The results can be broadly divided into two categories for the 1D and 2D cases. In the former, the variation along the lateral directions (x and y) is averaged; thus, every dependant variable is solely a function of the axial dimension (z). Balazs *et al.* adopted this approach in their studies of the PNC intercalation/exfoliation processes.[6] Unlike the 1D case, the 2D formulation only averages over one lateral dimension (y), while the variation in the x and z directions is considered. Thus, every dependent variable, e.g., volume fractions, probability functions, and excess free energy, has one additional degree of freedom.

A. The one-dimensional computations

Balazs *et al.* investigated a model PNC system of two infinitely large parallel platelets immersed in a bath of molten polymer.[5–10] The assumption of infinitely large platelets means that the system is translationally invariant in the x-y directions and the 1D calculations are fully adequate. For the translation invariance of dependant variables, our computations virtually reproduced their published results. Figure 2 illustrates the effect of the host polymer chain length in the range from 50 to 2000 Kuhn segments, i.e., corresponding to a molecular weight of PP up to ca. 500 kg/mol. The entropy and enthalpy contributions as well as the excess free energy are presented for the infinitely separated clay platelets. In

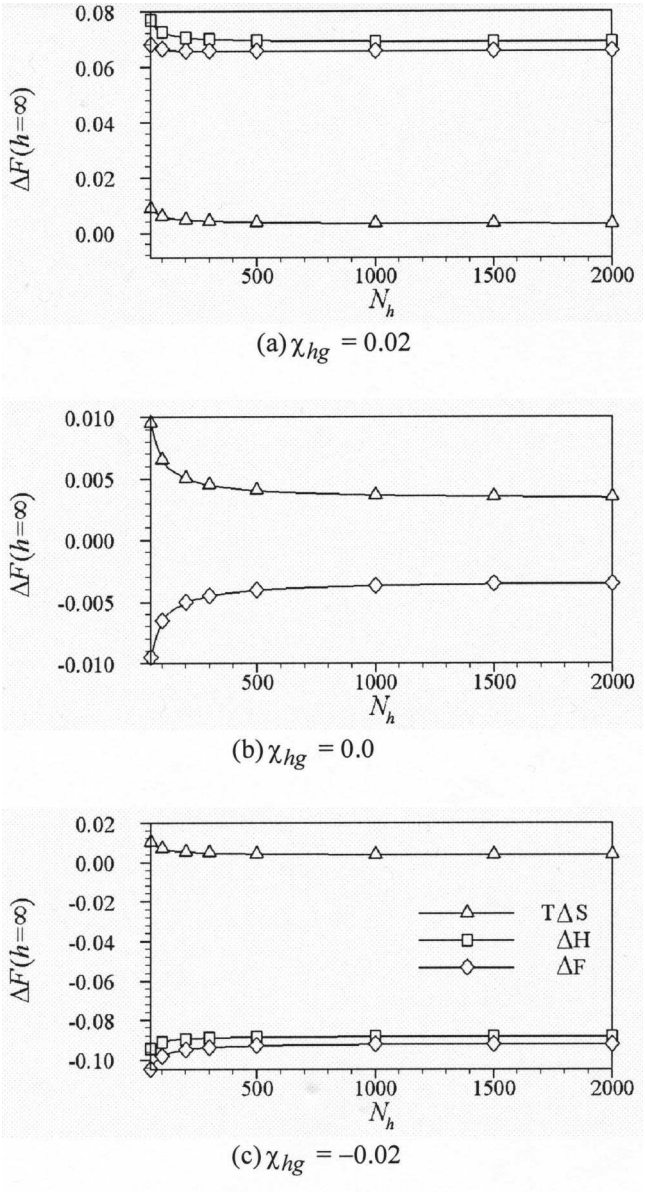

FIG. 2. Influence of the statistical chain length on excess free energy. $\rho_g=0.05$, $N_g=50$, $N_h\in[50,1000]$, and $\chi_{hg}\in[-0.02,0.02]$.

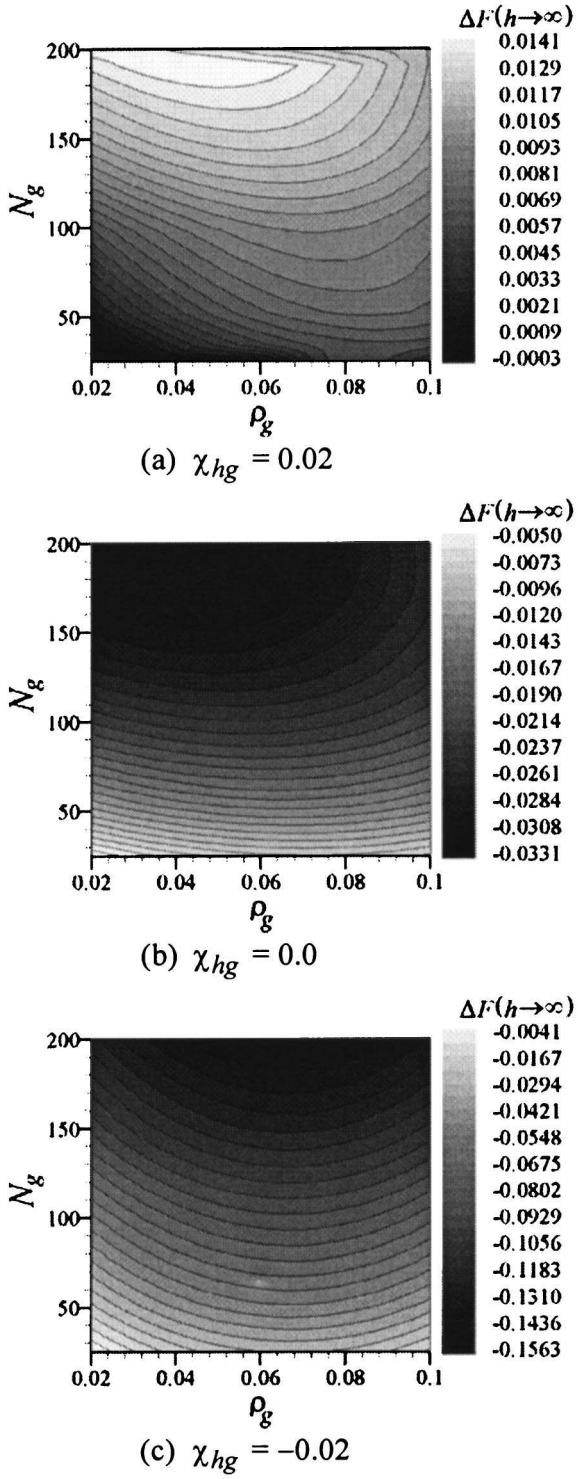

FIG. 3. Influence of the statistical chain length and grafting density on the asymptotic free energy $(h\to\infty)$. $N_h=200$, $N_g\in[25,200]$, $\rho_g\in[0.02,1]$, and $\chi_{hg}\in[-0.02,0.02]$.

Fig. 3, the optimal operational parameters are then identified for the various combinations of the grafting density and statistical chain length of the grafted polymer.

B. The two-dimensional computations

Here, the numerical implementation is further generalized incorporating the solid-solid and solid-liquid interactions based on the 2D formulation. The 2D approach gives rise to an extra constrain at both $x=1$ and M_x, as given in Eq. (21). Its influence is discussed in the following section. The 2D model also adopts different grafting schemes for the compatibilizer and organic modifier, e.g., variation of the grafting location, viz., center or edge, and a number of grafting sites. In the presence a of different bonding nature of the compatibilizer and organic modifier, the 2D approach can provide a more appropriate treatment for tethering different macromolecules on a clay surface. For example, a 4% surface occupancy may be concentrated in a single cell at the center, or it may be distributed overeach cell by 0.4% for each 10 lateral cells at $z=1$. Evidently, a different fabrication scheme results in a different level of excess free energy due to the different distance to the edge, where the bulk condition prevails.

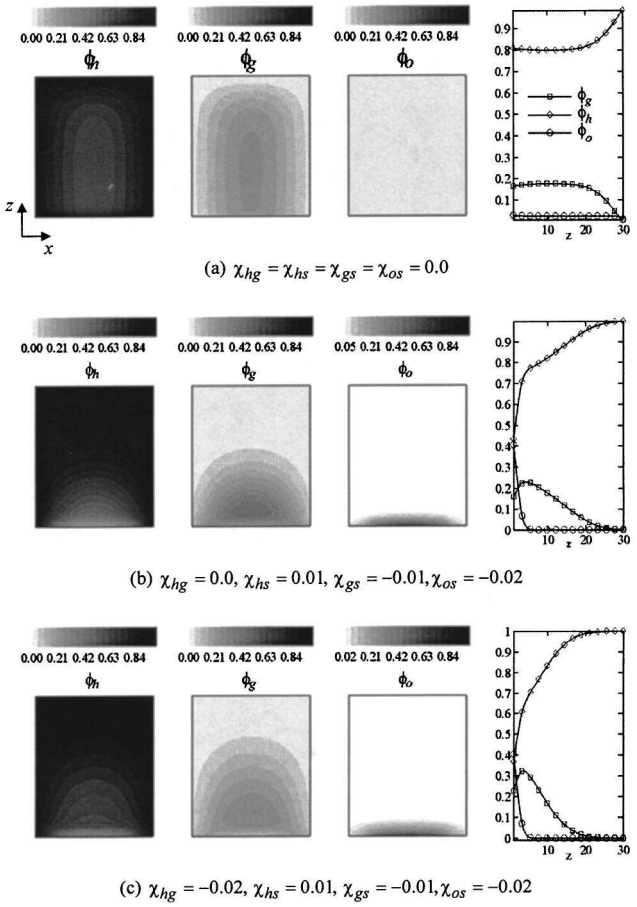

FIG. 4. Influence of the binary interaction parameters on the volume concentration profiles. $N_h=400$, $N_g=200$, $\rho_o=0.7$, $\rho_g=0.15$, and $\rho_h=0.05$.

Figure 4 displays the effect of the binary interaction parameters on the density profile for the host polymer, compatibilizer, intercalant, as well as the x-averaged fraction of all the three components. Three different sets of interactions are considered: mutually neutral (top), and then attractive for the clay with the intercalant and grafted polymer, but repulsive for the host polymer. In the latter situation, two types of interactions between the polymer and compatibilizer chains are considered: neutral (middle row) and slightly attractive (bottom row).

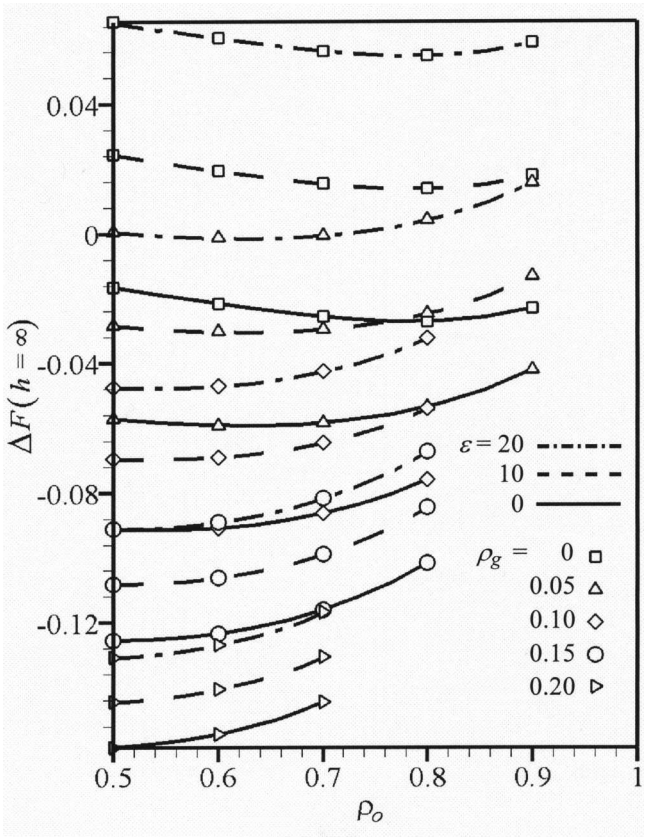

FIG. 5. Influence of the area-lattice ratio and grafting densities of the compatibilizer and intercalant on the asymptotic free energy ($h\to\infty$). $N_h=400$, $N_g=200$, $N_o=10$, $\rho_g\in[0,0.2]$, $\rho_o\in[0.5,0.9]$, $\epsilon\in[0,20]$, $\chi_{hg}=0.0$, $\chi_{hs}=0.01$, $\chi_{gs}=-0.01$, $\chi_{os}=-0.02$, and $A=20$.

The excess free energy as a function of the intercalant grafting density is shown in Fig. 5. Similar to the case in Fig. 4, here, the system also comprises of the host polymer, intercalant, compatibilizer, and clay. Five grafting levels of compatibilizing polymer were used. Furthermore, it was assumed that the magnitude of the solid-solid interaction is determined by the Hamaker constant A and the clay-segment surface ratio ϵ. Computations were performed for the constant chain length ($N_h=400$ and $N_g=200$) as well as the same set of the solid-liquid binary interaction parameters as in Fig. 4(b).

IV. DISCUSSION

While for the model consisting of infinite parallel platelets in molten polymer a 1D simulation is adequate, this may not be so if the platelets are of a finite size and the grafting locations vary with the distance from the edge. In a real PNC having clay platelets of finite sizes (e.g., thickness of ca. 1 nm and surface area ranging from 10×30 to 100×500 nm^2), the equilibrium free energy may be different at different locations, and the excess free energy may be different than that computed from the 1D model. Consequently, for the SCF computations in 2D, it was assumed that the clay platelets have a final width; hence, the property vary with the cell number in the x direction (properties in the y direction were assumed invariant). Thus, the assumption of two parallel platelets immersed in molten polymer bath is maintained, but these have a finite size, i.e., finite number of cells in the x direction. The 2D computations were carried out by assuming the Boltzmann distribution for both the axial (z) and lateral (x) directions.

A. One-dimensional SCF model without the solid-solid interaction

The "classical" 1D simulation for macromolecules at the interface was published by Fleer *et al.*[3] and for PNC by Balazs and her colleagues.[6–9] The initial SCF computations showed that at a constant grafting density, $\rho_g=0.04$, and at neutral interactions between intercalant and polymer, $\chi_{oh}=0.0$, the system was miscible and the miscibility increases with the intercalant chain length, $N_g\in[25-100]$. Furthermore, increasing the grafting density ρ_g was shown to reduce the free energy of mixing; thus, the system may become immiscible. In the latter publications,[9,10] a hybrid model of SCF with DFT was used to compute the phase diagrams for PNC. At a constant loading of grafted chains, $\theta=\rho_g$, $N_g=1$ or 2, and short chain length, $N_g=5$, the system was found immiscible for the Huggins-Flory parameter $\chi_{gh}\in[-0.05,0.05]$ and for a certain level of clay concentration. Furthermore, it was concluded that longer grafted chains enhance the steric stability and hence are more favorable.

The previous authors carried out most of their calculations for $N_g\leqslant100$ and $N_h=100$ Kuhn segments. However, Fig. 2 indicates that even for $N_h>1000$, both the enthalpy and entropy of mixing change. For the case of neutral interactions between the polymer and compatibilizer, the heat of mixing is absent, and the entropy of mixing dominates the free energy of mixing. By contrast, for the non-neutral interactions, the free energy is remarkably constant for $N_h>200$.

Figure 3 shows that an increase of grafting density does not always lead to an improved intercalation. The three figures display constant contours of $\Delta F(h\to\infty)$ for systems with attractive (bottom), neutral, and repulsive (top) interactions ($\chi_{hg}=-0.02$, 0.0 and 0.02). The figures show that for $\chi_{hg}=$constant, the optimum conditions for exfoliation depend on the grafting density and the compatibilizer chain length. The dark contours represent the negative value of $\Delta F(h\to\infty)$, favoring intercalation or exfoliation, whereas the white ones are the unfavorable conditions. For $\chi_{hg}=-0.02$, longer grafted polymer chains result in better dispersion. Within the range of the explored parameter values, the highest degree of clay dispersion should be obtained for $N_g=200$ and $\rho_g=0.07$. In the case where the compatibilizer is the end-grafted host polymer (hence, $\chi_{hg}=0.0$), the best dispersion is expected for $N_g=200$ but at a lower grafting density of $\rho_g=0.04$. The situation is notably different when the interactions are repulsive. The shortest chain length and smallest grafting density offer the best possibility for dispersion. The contour plots in Fig. 3 show the general behavior of ΔF in the asymptotic limit, when clay platelets are far apart: $h\to\infty$. However, as is evident from Figs. 4 and 6 in Ref. 6, ΔF variations, when the two platelets are in close proximity, are also of interest.

The effect of the grafting density on the aggregation of the grafted particles in a polymeric matrix was analyzed by

Ferreira *et al.* using a 1D SCF.[50] The authors demonstrated that the general scaling criterion for aggregation, hence immiscibility, in a three-component system (a surface, grafted component, and polymeric matrix) is $\rho_g\sqrt{N_g} > (N_g/N_h)^2$. However, in the four-component system of interest here, there is a two-step "brush" with a short intercalant and long compatibilizer chains. Thus, this criterion can be used only as a nonquantitative guide.

B. Two-dimensional SCF model with solid-solid interaction

In the 2D case, the variation along the lateral dimension, x direction, is no longer averaged; hence, the configuration schematically shown in Fig. 1 can be simulated. Furthermore, to bring the mathematical model closer to industrial reality, the system is assumed to comprise four components: relatively short chain intercalant (organic modifier), grafted polymer (compatibilizer or a coupling agent), host polymer, and inorganic clay platelets. The introduction of solid clay particles capable of interacting with all the other system components leads to novel results, which have not been reported in the literature and are not accessible from the 1D models.

In the preceding part, solid-solid and solid-liquid interactions were neglected. At present, interactions between all four components are treated using a 2D SCF model. Although the simulation can be carried out by varying several parameters (e.g., the same ones as considered in the 1D case, i.e., the statistical chain lengths, binary interaction parameters, and grafting density), the investigation focuses on the well-known PNC system, based on PP, containing organoclay and grafted PP as the compatibilizer (e.g., see Ref. 51). The main purpose of the 2D simulation is to identify the optimum values for the operational parameters at different levels of bare solid clay surface.

Figure 4 illustrates the effect of the binary interaction parameters on the concentration profiles of the host polymer (first column), grafted polymer (second column), and intercalant (third column) in a two-dimensional (x-z) lattice. The fourth column displays the x-averaged volume fraction of all the three components in the z direction. In this simulation, three types of molecules are sandwiched between a pair of clay platelets immersed in a reservoir of molten host polymer. Here, the solid-solid interactions are assumed absent, i.e., the clay platelets are fully covered by organic segments. The statistical chain lengths of the host polymer, grafted polymer, and intercalant were assumed as $N_h=400$, $N_g=200$, and $N_o=10$, respectively. The grafting density was taken as $\rho_h=0.05$, $\rho_g=0.15$, and $\rho_o=0.7$, thus leaving 10% of the clay sites ($z=0$) unoccupied initially. This vacancy, unlike ρ_v, will be occupied by any of the macromolecules throughout the interaction process. The size of the computational lattice was taken as $M_x=30$ and $M_z=10$. The computational domain consisted of a solid wall at $z=0$. The compatibilizer was assumed to be preferentially grafted at both edges of the plate ($x=1$, 2, 9, and 10), whereas the intercalant was uniformly spread over the clay platelet ($x=3\sim8$).

Figure 4(a) presents a trivial case where all the binary interaction parameters are neutral and the thermodynamics is solely determined by entropy. In this case, the placement of the constituents is controlled by the conformational potential (or hardcore repulsive potential u'). As the figure shows, the low mobility host polymer pushes the grafted polymer (compatibilizer) toward the central region—there is a strong separation between the two polymers suggesting immiscibility. The high mobility intercalant readily mixes with the two polymers but at the same time shows a small preference to the clay surface.

Figures 4(b) and 4(c) consider more realistic systems. Here, the presence of small attractive forces between clay and intercalant and between clay and grafted polymer are included. Furthermore, chemical bonding of one end of the intercalant and compatibilizer were incorporated—stronger for the ionically bonded intercalant than for the functionalized compatibilizer groups. A small repulsive interaction was postulated between the hydrophilic clay and hydrophobic host polymer. The figures display the density profiles for the two values of the homopolymer-compatibilizer interaction parameter—in Fig. 4(b), a neutral interaction between the two macromolecules was assumed ($\chi_{hg}=0$), whereas in Fig. 4(c), for the two polymers, an attractive interaction was considered ($\chi_{hg}=-0.02$).

It is evident from Figs. 4(a) and 4(b) that the simulation correctly predicts the increased concentration of the grafted copolymer as well as that of the intercalant near the solid wall. The assumption of an attractive interaction between the compatibilizer and the clay results in the contraction of the immiscibility region. The compatibilizer, for the case $\chi_{gs}=-0.01$ with grafting condition, occupies significantly a larger surface area, thus keeping away the host polymer with the unfavorable interaction with the clay ($\chi_{gs}=+0.01$). This is consistent with the computed behavior of the excess free energy of mixing. The neutral interactions between the end-tethered compatibilizer and host macromolecules provide little inducement for the grafted polymer to mix with the host polymer. Again, due to the high mobility and attraction to the surface, the intercalant strongly bonds to the surface. Thus, a slight gain of the concentration profile is found at $z=4$. Noteworthy is that the concentration profiles in Figs. 4(b) and 4(c) are similar.

Comparison of Figs. 4(b) and 4(c) demonstrates the effect of the small attractive interactions between the host and grafted polymer on the concentration profiles. Evidently, the attractive interactions improve the miscibility between the two polymers, thus greatly reduce the central zone of immiscibility—a small region of high compatibilizer concentration remains near the central region ($x=5$). Furthermore, the rate of concentration decrease in Fig. 4(c) is reduced, indicating better miscibility between the host polymer and compatibilizer than that in Fig. 4(b). The averaged volume profile can be further compared with Fig. 5 in Ref. 6. In the presence of a strong intercalant concentration, the profiles for the host polymer and compatibilizer favorably interacting with each other ($\chi_{hg}=-0.02$) do not show a broad range of overlap as mentioned in Ref. 6. The gain in the concentration profile for a compatibilizer is observed at $z=4$, going from Figs. 4(b)–4(c). These profiles may be compared with the data displayed in Fig. 5 of Ref. 6. Both Figs. 4(b) and 4(c)

show a relatively sharp increase in ϕ_h and a steep decrease in ϕ_o, indicating the influence of the extra bulk condition at $x=1$ and M_x in lateral dimension (x direction).

In their study of the effects of the statistical chain length and grafting density, Balazs *et al.*[6–9] observed that the magnitude of the binary interaction parameter between two polymers with a short statistical chain length has a relatively small effect on exfoliation. By contrast, the effect is quite pronounced for relatively long polymer chains. The important effect of molecular weight has been recognized in the theories of polymer solutions ($\propto \chi_{12} N^{1/2}$) and polymer blends ($\propto \chi_{12} N$).[32] However, a high molecular weight compatibilizer is beneficial in systems with good miscibility between the host polymer and the main chain of the grafted polymer, i.e., for $\chi_{hg}<0$, and detrimental for systems where $\chi_{hg}>0$. To reach these conclusions, several simplifying assumptions had to be made, e.g., that the clay platelets are fully covered by a short chain organic intercalant and that the interactions with bare solid clay platelet can be neglected.

Figure 5 shows the plot of the asymptotic free energy of mixing, $\Delta F(h\to\infty)$, as a function of the intercalant grafting density ρ_o. The graph was generated (see Table I) assuming that $N_h=400$, $N_g=200$, and $N_o=10$. The same set of the binary interaction parameters, as in the case of Fig. 4(b) was used; $\chi_{hs}=0.01$, $\chi_{gs}=-0.01$, and $\chi_{os}=-0.02$. Thus, it was assumed that no favorable interaction exists between the host polymer and the compatibilizer chain. The computations based on Eqs. (15) and (16) were carried out for five levels of the compatibilizer grafting densities, $\rho_g\in[0,0.2]$. For the solid-solid interactions, the value of the Hamaker constant was taken as $A=20\,(k_BT)$, while the clay-lattice surface ratio in Eq. (9) was $\epsilon\in[0,20]$.

In the absence of solid-solid interactions ($\epsilon=0$), the free energy of mixing ΔF is negative, decreasing with the compatibilizer grafting density ρ_g, hence, indicating increasing miscibility of the system with the compatibilizer content. Furthermore, for $\rho_g=0$, there is a shallow, local minimum indicating more favorable conditions for the specific balance of the intercalant and copolymer concentrations. The presence of local minima was also noted from the 1D model (see Figs. 4(b) and 6 in Ref. 6). As the compatibilizer grafting density increases, ΔF decreases, but the decrease is significantly smaller at higher intercalant grafting density, $\rho_o>0.6$.

In the presence of solid-solid interactions ($\epsilon=20$), the values of $\Delta F(h\to\infty)$ range from strongly positive to strongly negative. At a low compatibilizer concentration, $\rho_g\leqslant 0.05$, ΔF is positive, indicating immiscibility of the system. At higher compatibilizer grafting densities, $\rho_g>0.05$, ΔF is negative, decreasing with ρ_g—the system is miscible. However, the efficiency of the compatibilizer decreases with increasing the values of both ρ_g and ρ_o.

When a lower value of the solid-solid interactions was assumed ($\epsilon=10$), the free energy of mixing, $\Delta F(h\to\infty)$, showed an intermediate behavior—in the absence of the compatibilizer, the system was immiscible, but $\rho_g<0.05$ was sufficient to change the sign. At higher compatibilizer loadings, ΔF became the same for $\epsilon=10$, as for $\epsilon=0$, the easiest exfoliation is expected when $\rho_g=0.20$ and $\epsilon=0$ or 10. Thus, the simulation indicates that the presence of a sufficient amount of compatibilizer prevents the bare clay platelets from interacting with each other or with the host polymer and effectively removes these unfavorable contributions to ΔF. This trend is further confirmed by comparing the density profiles for systems with solid-solid interactions containing different amounts of grafted polymer. For example, the difference in excess free energy between the solid and dashed lines, $\epsilon=0$ (no solid interactions) and $\epsilon=10$, respectively, at $\rho_g=0.0$ is rather large but diminishes at higher ρ_g values.

The effect of increasing the intercalant grafting density is dual; on the one hand, it prevents the host polymer from unfavorably interacting with the solid platelet but on the other, it also prevents the favorable interactions of the compatibilizer with the clay. For practical reasons, a minimum amount of compatibilizer should be used in the system with fractional bare surface, e.g., at $\epsilon=10$. As the results in Fig. 5 indicate, the optimum intercalant grafting density is about $\rho_o=0.6$ to 0.7. This indicates that the concentration of the grafted intercalant and compatibilizer must be carefully balanced.

V. SUMMARY, CONCLUSION, AND OUTLOOK

The adopted SCF simulation methodology is an extension of the work of Balazs *et al.*[6–9] To bring the model closer to practical industrial strategies for the preparation of PNC, four components have been considered: solid clay lamellae, short-chain intercalant, long-chain end-functionalized compatibilizer, and host polymer. Accordingly, three types of interaction parameters were used in the simulations: solid-solid, solid-liquid, and liquid-liquid. Realistic values of the short and long-range binary interaction parameters were selected from the literature.

The initial one-dimensional simulations were carried out to confirm the accuracy of the new simulation model and computational methodology. Good agreement was found with the results in the literature for simple system.[6] In the next step, the 1D model was extended to four components including the crystalline solid lamellae characterized by high surface potential. Finally, the computations were performed for the 2D lattice model. These results were slightly different (and intuitively more realistic) than those obtained for the 1D. The motivation for the inclusion of the solid platelet interactions was provided by the well-known thermal instability of organoclays under normal polymer processing conditions, which leads to the progressive removal of the intercalant from the clay surface, often resulting in the reaggregation of the platelets.[1,52]

Using the one-dimensional model (without the solid surface present), the simulation successfully identified the optimum range of the operational parameters such as the grafting density and the statistical chain length of a compatibilizer macromolecule for the three values of the binary interaction parameters between the host and compatibilizer polymer chains, χ_{hg}. Results of the application of the methodology to real system, viz., fully preintercalated organoclay with polypropylene (PP) and end-functionalized PP as compatibilizer (i.e., $\chi_{hg}=0$), suggest that for the best performance, about

4% of the clay sites should be reacted with a compatibilizer of similar molecular weight (MW) as that of PP.

In the 2D model, the effects of solid-solid and solid-liquid interactions were examined in addition to the previously studied variables. The limited 2D results successfully reproduced those of the 1D formulation. In addition, they demonstrated the strong influence of the solid-solid interactions. In the absence of the compatibilizer, even with only 2% (surface fraction) bare surface, the system was found to be thermodynamically immiscible. Hence, organoclay exfoliation would not be expected.

The neutral interaction case exhibits a limited range of intercalation, only if more than 5 vol % compatibilizer is added for $\epsilon=20$. For the mentioned PP system, the compounding strategy must focus on the minimization of the bare clay surface (e.g., as caused by the thermal decomposition of the intercalant during compounding or extraction by the molten polymers), and the use of the few high MW compatibilizing macromolecules, as suggested in literature.[6] Evidently, the dispersion would be improved if some attractive interactions between the host and compatibilizer chain polymer could be developed, i.e., $\chi_{hg}<0$. This system can be realized in PNC with miscible polymer blends. For example, PNC with polyphenylene ether as the host polymer compatibilized with the end-terminated PS. Unfortunately, for the PP matrix, such a strategy is not likely to be readily available.

The two-dimensional model with four contributing components indicates that, in the presence of a small percentage of solid surface ($\epsilon=10$), the minimum amount of compatibilizer to secure the miscibility of the system is $\rho_g=0.03$ to 0.05 and that of the intercalant is about $\rho_o=0.6$ to 0.7. Exfoliation would be easier for higher values of ρ_g but at a higher PNC cost.

The few examples of the simulation results illustrate the usefulness of this approach as a guiding tool for solving difficult practical problems. However, there are serious limitations imposed by the idealized models. Of these, four are probably the most important.

(1) The use of realistic values of MW and interaction parameters χ. The problem is far from trivial considering the polydispersity of MW, presence of additives, and thermodynamic nonequilibrium conditions experienced during compounding. Furthermore, the binary interaction parameter is a misnomer—in reality, χ_{ij} is a complex function of many independent variables!

(2) Extension of the present computer code to three dimensional (3D) would bring the simulation still closer to reality. Noteworthy is that as the comparison of the 1D with the 2D results indicates, the entropic contribution in higher dimensionality improved the miscibility especially in the marginal miscibility situations. Thus, the 3D code may also lead to different results.

(3) The present use of two platelets in the infinite reservoir of molten polymer prevents the use of a solid concentration as an independent variable. Furthermore, the obtained simulation results indicate the potential miscibility/immiscibility at an infinite dilution. However, the developed code can readily be extended to the practical concentration range.

(4) The lattice models impose constraints absent in the molecular dynamic (MD) formalisms. However, the latter are still limited in the number of elements and dimensions they can consider. There are also problems with the common assumption of the SCF model that the binary interaction parameters are constant and quite arbitrary in magnitude. Hybridization of the SCF with MD may offer the best approach for calculating the equilibrium free-energy changes with gap expansion. A more ambitious goal would be to compute the full phase diagrams, similarly as these are computed from the SCF+DFT hybrid.[10] Hybridization of the different length scale methodologies in 3D, e.g., MD, SCF, and continuum mechanics, offer intriguing potentials for predicting PNC morphology and performance.

ACKNOWLEDGMENT

This work has been supported by NSERC strategic grant for the McGill/IMI project.

[1] L. A. Utracki, *Clay-Containing Polymeric Nanocomposite, Monograph* (Shrewsbury, UK, in press).
[2] A. Maczek, *Statistical Thermodynamics* (Oxford University Press, New York, 1998).
[3] G. J. Fleer, M. A. Cohen Stuart, J. M. H. M. Scheutjens, T. Cosgrove, and B. Vincent, *Polymers at Interfaces* (Chapman & Hall, London, 1993).
[4] R. A. Vaia and E. P. Giannelis, Macromolecules **30**, 7990 (1997).
[5] R. A. Vaia and E. P. Giannelis, Macromolecules **30**, 8000 (1997).
[6] A. C. Balazs, C. Singh, and E. B. Zhulina, Macromolecules **31**, 8370 (1998).
[7] E. B. Zhulina, C. Singh, and A. C. Balazs, Langmuir **15**, 3935 (1999).
[8] C. Singh and A. C. Balazs, Polym. Int. **49**, 469 (2000).
[9] A. C. Balazs, V. V. Ginzburg, and Y. Lyztskaya, in *Modeling the Phase Behavior of Polymer-Clay Nanocomposites*, edited by T. J. Pinnavaia and G. W. Beall (Wiley, New York, 2000).
[10] V. V. Ginzburg, A. C. Balazs, and C. Singh, Macromolecules **33**, 1089 (2000).
[11] J. Y. Lee, A. R. C. Baljon, R. F. Loring, and A. Z. Panagiotopoulos, J. Chem. Phys. **109**, 10321 (1998).
[12] A. R. C. Baljon, J. Y. Lee, and R. F. Loring, J. Chem. Phys. **111**, 9068 (1999).
[13] J. Y. Lee, A. R. C. Baljon, and R. F. Loring, J. Chem. Phys. **111**, 9754 (1999).
[14] J. Y. Lee, A. R. C. Baljon, D. Y. Sogah, and R. F. Loring, J. Chem. Phys. **112**, 9112 (2000).
[15] R. A. Vaia, K. D. Jandt, E. J. Kramer, and E. P. Giannelis, Macromolecules **28**, 8080 (1995).
[16] E. Hackett, E. Manias, and E. P. Giannelis, J. Chem. Phys. **108**, 7410 (1998).
[17] J. S. Smith, D. Bedrov, and G. D. Smith, Compos. Sci. Technol. **63**, 1599 (2003).
[18] A. Sinsawat, K. L. Anderson, R. A. Vaia, and B. L. Farmer, J. Polym. Sci., Part B: Polym. Phys. **41**, 3272 (2003).
[19] F. W. Starr, T. B. Schroeder, and S. C. Glotzer, Phys. Rev. E **64**, 021802 (2001).
[20] M. Vacatello, Macromol. Theory Simul. **13**, 30 (2004).
[21] V. V. Ginzburg, O. V. Gendelman, and L. I. Manevitch, Phys. Rev. Lett. **86**, 5073 (2001).
[22] O. V. Gendleman, L. I. Manevitch, and O. L. Manevitch, J. Chem. Phys. **199**, 1066 (2003).
[23] K. Binder, *Monte Carlo and Molecular Dynamics Simulations in Polymer Science* (Oxford University Press, New York, 1995).
[24] D. A. McQuarrie and J. D. Simon, *Physical Chemistry: A Molecular Approach* (University Science Books, California, 1997).
[25] P. E. Rouse, J. Chem. Phys. **21**, 1272 (1953).
[26] P. G. De Gennes, *Scaling concepts in Polymer Physics* (Cornell University Press, New York, 1979).
[27] M. Doi and S. F. Edwards, *The Theory of Polymer Dynamics* (Academic, New York, 1986).
[28] B. H. Zimm, J. Chem. Phys. **24**, 169 (1956).

[29] O. F. Olaj, T. Petrik, and G. Zifferer, J. Chem. Phys. **108**, 8214 (1998).
[30] J. T. Padding and W. J. Briels, J. Chem. Phys. **118**, 10276 (2003).
[31] R. E. Rudd and J. Q. Broughton, Phys. Status Solidi B **217**, 251 (2000).
[32] L. A. Utracki, in *Polymer Blends Handbook*, edited by L. A. Utracki (Kluwer Academic Publishers, Dordrecht, 2002), Chap. 2.
[33] O. A. Evers, J. M. H. M. Scheutjens, and G. J. Fleer, Macromolecules **23**, 5221 (1990).
[34] O. A. Evers, J. M. H. M. Scheutjens, and G. J. Fleer, J. Chem. Soc., Faraday Trans. **86**, 1333 (1990).
[35] J. Genzer, Adv. Colloid. Interface Sci. **94**, 105 (2001).
[36] B. Van Lent, R. Israels, J. M. H. M. Scheutjens, and G. J. Fleer, J. Colloid Interface Sci. **137**, 380 (1990).
[37] T. Cosgrove, T. Heath, B. Van Lent, F. Leermakers, and J. M. H. M. Scheutjens, Macromolecules **20**, 1692 (1987).
[38] S. T. Milner, T. A. Witten, and M. E. Cates, Macromolecules **21**, 2610 (1988).
[39] C. M. Wijmans, J. M. H. M. Scheutjens, and E. B. Zhulina, Macromolecules **25**, 2657 (1992).
[40] X. Y. Li and D. L. Zhao, J. Chem. Phys. **117**, 6803 (2002).
[41] X. Y. Li and D. L. Zhao, J. Chem. Phys. **119**, 3996 (2003).
[42] F. Schmid, J. Phys.: Condens. Matter **10**, 8105 (1998).
[43] C. A. Tyler and D. C. Morse, Macromolecules **36**, 8184 (2003).
[44] T. Shima, H. Kuni, Y. Okabe, M. Doi, X.-F. Yuan, and T. Kawakatsu, Macromolecules **36**, 9199 (2003).
[45] P. J. Flory, *Statistical Mechanics of Chain Molecules*, 2nd ed. (Oxford University Press, New York, 1988).
[46] J. Vial and A. Carré, Int. J. Adhesion Adhesive **11**, 140 (1991).
[47] V. Médout-Marere, J. Colloid Interface Sci. **228**, 434 (2000).
[48] L. A. Utracki, R. Simha, and A. Garcia-Rejon, Macromolecules **36**, 2114 (2003).
[49] J. J. Moré, D. C. Sorensen, K. E. Hillstrom, and B. S. Garbow, The MINPACK Project, in *Sources and Development of Mathematical Software*, edited by W. J. Cowell (Prentice-Hall, Englwood Cliffs, 1984).
[50] P. G. Ferreira, A. Ajdari, and L. Leibler, Macromolecules **31**, 3994 (1998).
[51] N. Hasegawa and A. Usuki, J. Appl. Polym. Sci. **93**, 464 (2004).
[52] S. Tanue, L. A. Utracki, A. Garcia-Rejon, P. Sammut, M-T. Ton-That, I. Pesneau, M. R. Kamal, and J. Lyngaae-Jörgensen, Polym. Eng. Sci. **44**(6), 1061 (2004).